ORIGINAL ARTICLE

Quantitative SPECT/CT: SPECT joins PET as a quantitative imaging modality

Dale L. Bailey · Kathy P. Willowson

Abstract The introduction of combined modality single photon emission computed tomography (SPECT)/CT cameras has revived interest in quantitative SPECT. Schemes to mitigate the deleterious effects of photon attenuation and scattering in SPECT imaging have been developed over the last 30 years but have been held back by lack of ready access to data concerning the density of the body and photon transport, which we see as key to producing quantitative data. With X-ray CT data now routinely available, validations of techniques to produce quantitative SPECT reconstructions have been undertaken. While still suffering from inferior spatial resolution and sensitivity compared to positron emission tomography (PET) imaging, SPECT scans nevertheless can be produced that are as quantitative as PET scans. Routine corrections are applied for photon attenuation and scattering, resolution recovery, instrumental dead time, radioactive decay and cross-calibration to produce SPECT images in units of kBq.ml^{-1}. Though clinical applications of quantitative SPECT imaging are lacking due to the previous non-availability of accurately calibrated SPECT reconstructions, these are beginning to emerge as the community and industry focus on producing SPECT/CT systems that are intrinsically quantitative.

Keywords SPECT · Quantitative

D. L. Bailey
Department of Nuclear Medicine, Royal North Shore Hospital,
Faculty of Health Sciences,
University of Sydney, Sydney, Australia

D. L. Bailey (✉)
Department of Nuclear Medicine, Royal North Shore Hospital,
St Leonards, NSW 2065, Australia
e-mail: dale.bailey@sydney.edu.au

K. P. Willowson
Department of Nuclear Medicine, Royal North Shore Hospital,
School of Physics,
University of Sydney, Sydney, Australia

Introduction

The measurement of radionuclide distribution remains one of the few truly quantitative in vivo imaging tools available. Measurements with MRI or X-ray CT of in situ tissue constituents such as proton or electron density, or after the injection of a contrast agent, do not have the same quantitative potential to measure physiology and biochemical processes as do the nuclear medicine techniques of single photon emission computed tomography (SPECT) and positron emission tomography (PET). From its inception, PET systems have been developed that are intrinsically capable of producing cross-sectional images in units of kBq.ml^{-1}. In this regard, PET has been greatly assisted by the simplicity of correcting for photon attenuation within the body. SPECT, on the other hand, is not as readily amenable to correction for photon attenuation due to the differences in the basic physics of measuring a single photon compared to the dual photon coincidence detection strategy employed in PET. For this reason the dogma has emerged that "PET is quantitative, but SPECT is not". Evidence to support this statement can be found as recently as last year in an article where the authors made the statement that "…*PET is superior to SPECT in both sensitivity and spatial resolution. Furthermore, PET enables quantitation* [sic] *of tissue radioactivity concentrations*" [1].

Today, technological advances have brought the goal of producing quantitative SPECT images for clinical use closer to realisation. These advances include:

- Ready availability of co-registered CT data for use in attenuation correction (AC) and scatter correction (SC) schemes.
- Improved digitised detector performance plus mechanical and electronic stability.
- Improved reconstruction algorithms that can incorporate the underlying physics into the image formation process unlike the filtered back-projection algorithm.

- Ever-increasing computational power in the desktop environment that allows sophisticated algorithms to be implemented and used clinically.
- Finally, continuing increased utilisation of PET/CT which has demonstrated the clinical potential of quantitative radionuclide imaging, encouraging renewed interest in producing similar measures with SPECT.

In this paper we will discuss the necessary corrections and requirements for producing quantitative SPECT images and the current limitations on the results achievable.

Requirements for quantitative emission tomography

Historically, SPECT and PET imaging emerged at approximately the same time in the late 1970s. SPECT cameras were based on modified gamma cameras that could rotate about the subject to acquire 360° of data and rapidly found a role in clinical nuclear medicine. PET, however, firmly remained a research device as the tomographs continued to develop over the next 20 or so years before they became the invaluable tool that they are today in the management of patients with cancer. In terms of their quantitative capability, the potential for PET was emphasised from the outset whilst in SPECT it has taken longer to develop. The reasons for this include (a) correction for photon attenuation of the dual photons emitted in the annihilation process and coincidence detection in PET could be readily determined from a radionuclide transmission scan and easily implemented, (b) that the early PET tomographs were strictly 2D, transaxially oriented multi-slice acquisition systems with very little acceptance of scattered photons within the imaging plane and hence no need for scatter correction, and (c) the research-oriented nature of early PET studies placed more emphasis on quantitatively accurate images to use in, for example, tracer kinetic modelling of tissue response curves using arterial blood concentrations of the radiopharmaceutical as the input function for the analysis, and thus all counters and tomographs had to be calibrated in the same units, namely radioactivity concentration per unit volume ($kBq.ml^{-1}$). In contrast, SPECT systems were more challenging to apply attenuation correction with, contained a relatively high fraction of scattered photons in the photopeak window (30–40 % in a typical ^{99m}Tc study) leading to the necessity for scatter correction algorithms and the clinical orientation of most SPECT studies performed with the associated need for a rapidly available scan report precluded spending long periods of time applying advanced processing techniques to produce quantitative SPECT reconstructions. In addition, SPECT is further complicated by the necessity for modelling and testing of corrections at differing photon energies (and photopeaks and collimators) corresponding to each radionuclide being used, as opposed to the constant 511 keV annihilation

photon energy consistent across all PET studies, regardless of the radionuclide. In short, SPECT scans have been traditionally interpreted without any correction for attenuation or scattering of the photons. This has led to clinicians "learning to read around" certain effects in the reconstructed images such as "attenuation artefacts" in myocardial perfusion imaging, particularly in the inferior and septal walls of the left ventricle.

Today, there is a greater degree of similarity between SPECT and 3D PET when it comes to the need for producing quantitatively accurate images: both require corrections for photon attenuation and scattering (scattered events now accounting for ≥40 % in 3D PET systems), uniformity of detector response, detector dead time, radionuclide decay, etc. Table 1 compares a number of the corrections applied to SPECT and PET data to ensure quantitative accuracy and compares the implementation in each modality.

Correction for photon attenuation

One of the main differences between SPECT and PET is the manner by which emitted photons are attenuated. In SPECT, the detected photon event rate is a combination of both the unknown strength of each individual point source emitter of gamma photons and the (usually unknown) attenuation through the object from source to detector. In Fig. 1 the image representing the SPECT situation demonstrates that a highly radioactive source, located deep within the object, and passing through a large amount of unknown attenuation may result in a similar count rate seen by the detector as a low activity source passing through very little attenuating media. In contrast, the image on the right in Fig. 1 representing the PET situation shows the two photons emitted after positron annihilation both passing through the full cross-sectional thickness of the body before being detected. The counting rates seen by the detectors in this situation would reflect the differences in the strength of each of the radioactive sources. Further, in PET it can be shown that the count rate detected is *independent* of the position of the source along the particular line of response. Thus the measurement of the transmission factor from an external source along each line of response gives an exact correction factor for that particular path. In contrast, the SPECT signal is a composite of the two unknowns of radioactive source strength and total attenuation combined into one overall count rate. From this single measurement it is not possible to separate the SPECT data into source strength and source depth/attenuation factor, unlike the case in PET where the detected signal strength is independent of the source depth.

Correction for photon attenuation in SPECT, therefore, relies on approximate solutions. One of the first implementations of an approximate algorithm for photon attenuation correction using filtered back-projection image reconstruction for SPECT was from Chang [2]. In this method, the emission source distribution was assumed to be contained within a

Table 1 Parameters affecting quantitative SPECT and PET image formation

Parameter	SPECT solution	PET solution	Comment
Photon attenuation	CT-based AC	CT-based AC	PET AC is applied in projection space prior to reconstruction; SPECT AC is applied during the reconstruction process (in OSEM)
Photon scattering	Mostly energy window based—some CT-based methods now	CT-based SC	In PET most tomographs use "single scatter approximation", whereas in SPECT a number of different approaches are used
Dead time correction	Usually applied as a scalar from a priori experiments	Usually measured in real time at detector level in each patient study	Dead time correction in SPECT is typically <10 %, whereas in PET it can be much greater due to high (e.g. MHz) single photon flux on detectors
Reconstruction algorithm	2D OSEM	3D OSEM	Both use same general approach today
Distance-dependent resolution variation	Measure actual radius of rotation of detectors as they rotate about subject and apply correction	Fixed ring geometry so can measure or estimate point-wise variation in spatial resolution	Both applied during reconstruction process
Decay correction and branching ratio of radionuclide	Historically not usually implemented on SPECT systems	Routinely applied to PET systems	Dependent on dose calibrator used and correct cross-calibration with tomograph
System sensitivity	Not usually implemented but can be experimentally determined and applied post-reconstruction	Inherently included as scaling factor in DICOM data	Relies on cross-calibration with dose calibrator

OSEM ordered subset expectation maximisation

uniform, homogeneously attenuating object. The correction term for each pixel is calculated as the average attenuation to the pixel, using a constant attenuation coefficient (μ) for the attenuation map (Fig. 2).
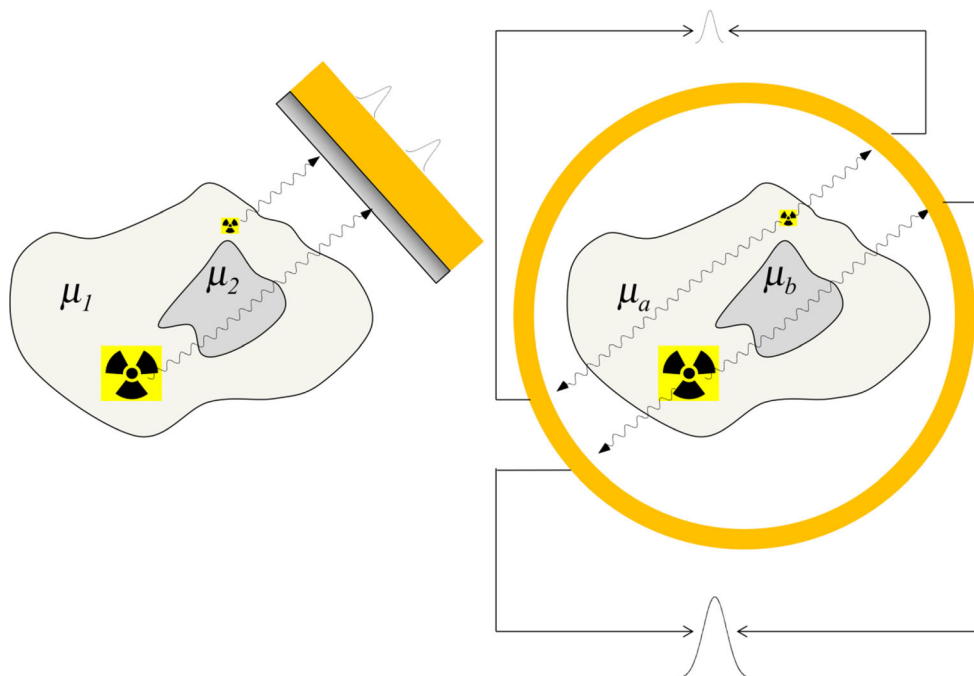

Fig. 1 In SPECT (schematically shown in *left image*) the detector (represented by the *orange shaded area*) may be unable to distinguish between a highly radioactive source (indicated by the radioactive 'trefoil' icon) at a greater depth in the body from a less radioactive source situated near the periphery, with less attenuation. Both situations could result in an identical photon flux (count rate). In PET, however (*right image*), as two photons are emitted and have to traverse the full thickness of the body before being measured in coincidence the differences in source strength will be reflected in the detected photon flux. In addition, it does not matter where the sources are located in the body along any particular line of sight as the count rate will remain the same independent of source location for that photon path

Using an iterative approach the reconstruction obtained for the attenuation corrected radionuclide distribution is forward-projected and compared with the measured projection data. Differences between the two images are found by subtraction and then back-projected to try and achieve a reconstruction that more closely matches the measured data. It is of note that this method did not utilise any transmission measurements but performed best when an accurate body contour was employed—which could be potentially found from the object boundary seen on the projection data. The "Chang correction" has been implemented in most commercially available systems that provide SPECT reconstruction. It is usually configured to use a constant attenuation coefficient (μ value) within an elliptical object boundary approximating the body. A more advanced approach is to employ the Chang algorithm using measured attenuation coefficients rather than assuming a constant homogeneous attenuation value [3]. An example is shown in Fig. 3. Attenuation correction can also be included in the transition matrix of an iterative reconstruction algorithm such as the expectation maximisation maximum likelihood (EMML) method [4] or its block-iterative implementation known as ordered subset expectation maximisation (OSEM) [5].

Initially, attenuation data were obtained using the gamma camera with radionuclide transmission sources such as ^{57}Co and ^{153}Gd [6]. Today, however, these have been replaced by the use of X-ray CT scans as initially investigated by Moore and others since the early 1980s [7–9]. The inclusion of measured transmission data, from either radionuclide-based techniques or from X-ray CT, is seen as the key to implementing quantitative SPECT.

The use of X-ray CT data for radionuclide attenuation correction requires the CT scan, usually represented in Hounsfield units (HU) related to the attenuation coefficients and the electron density, be converted into appropriate attenuation factors for the radionuclide being imaged [10]. The measured transmission factors used in reconstructing the CT data differ greatly from the attenuation of the gamma photons emitted by the radionuclide. Firstly, the X-ray photons are much lower energy than most of the radionuclide gamma photons that are used. Secondly, the energy spectrum for the X-rays are polychromatic and are composed of characteristic X-rays due to discrete energy transitions between different electron shells in the target of the X-ray tube superimposed on a continuous background spectrum of bremsstrahlung radiation, while the radionuclide photons emitted are of discrete energies. Due to this difference in the energy and nature of the energy spectra the X-ray photons are predominantly absorbed by the photoelectric effect, whereas the gamma photons interact with matter principally by the Compton scattering effect. In essence, these differences mean that a simple scaling from CT Hounsfield numbers to appropriate attenuation factors is not possible.

A number of studies have demonstrated that the conversion from CT numbers to the attenuation coefficients demonstrates a bilinear nature [10, 12–15]. Typically, for a CT number of less than ~0 HU a simple linear regression can be applied to convert the data, whereas above this value a different regression equation is required. As might be expected the higher the gamma photon energy the greater the difference in the slopes of the two components of the conversion. This can be seen in the graph of data from our laboratory in Fig. 4. Using a threshold technique, the CT scan is separated into two images defined by the cut-off where the bilinear regression changes from one regression equation to the other. The process for implementing this conversion from HU to μ map is shown in Fig. 5. The final step in the process of producing the radionuclide-specific attenuation map is to blur the map to approximately match the spatial resolution of the SPECT scan. This is done to avoid introducing sharp edges in the reconstructed SPECT images propagated

Fig. 2 The calculation of the attenuation correction factor (*ACF*) from the μ map is shown. Transmission factors are calculated for every point (x,y) inside the object for a number of angles over 360° and averaged. The inverse of this average attenuation factor is the attenuation correction factor term $A(x,y)$. The attenuation correction factors are generally highest towards the centre of the object

"μ map" - μ(x,y)   Chang ACF map - A(x,y)
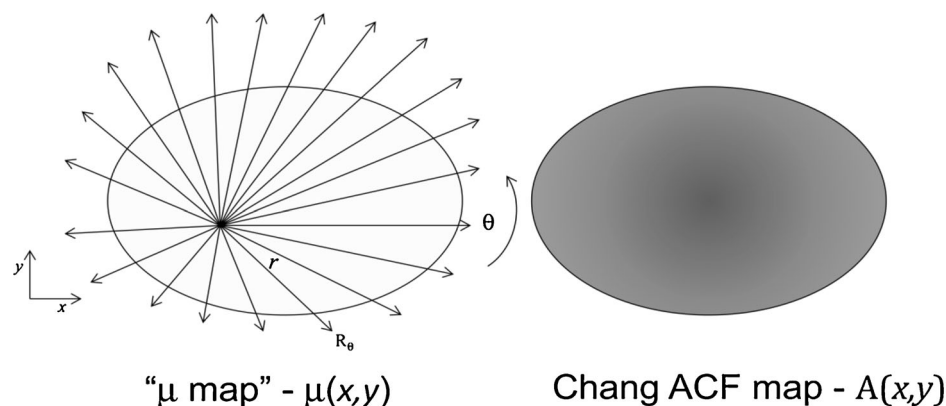
$$A(x,y) = \left\{ \frac{1}{2\pi} \sum_{\theta=0}^{2\pi} \sum_{r=0}^{R_\theta} exp\{-\mu(r)\}\Delta r \right\}^{-1}$$
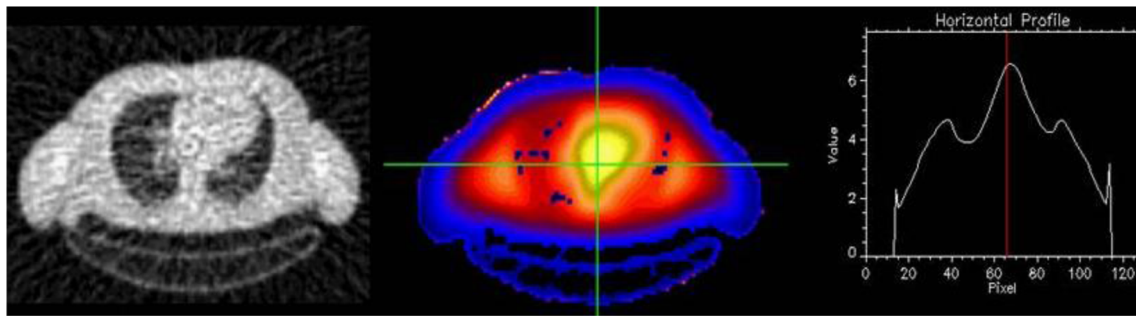
Fig. 3 The attenuation map shown on the *left*, measured with radionuclide sources, produces the Chang correction factor map [A(x,y)] for ^{99m}Tc photons in the *centre*. The profile using the cross hairs across from the attenuation map. Any metallic objects present in the image in the graph on the *right* shows the variation in the correction factors with a peak towards the centre of approximate sevenfold

from the attenuation map. Any metallic objects present in the body, such as dental fillings, prosthetic joints, etc., may lead to artefactually high attenuation coefficients and need to be considered for the impact that may be caused locally on the reconstructed emission radioactivity concentration.

After the attenuation map is obtained it can then be used either in the image reconstruction process or applied as a post hoc correction (modified Chang method). Correcting for attenuation using a co-registered CT scan, as opposed to assumed attenuation coefficients or a radionuclide-based transmission measurement, greatly assists the production of quantitative images of the SPECT data.
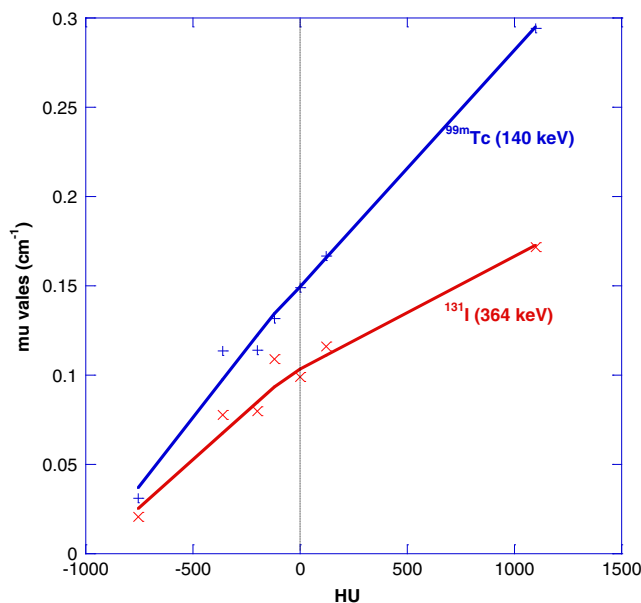

Fig. 4 Example data from our laboratory demonstrating the bilinear nature of the conversion from CT numbers (x-axis) to linear attenuation coefficient (y-axis) for the radionuclides ^{99m}Tc and ^{131}I are shown. The change in the regression equation is applied at HU=0. The data were obtained on a single slice CT scanner (PQ5000, Philips) and a dual detector gamma camera (Philips Medical Systems) [11]

Correction for scattered photons

The correction for scattered photons in SPECT imaging has been the subject of investigation for a considerably longer period than it has in PET imaging. When measuring the distribution of ^{99m}Tc in a human, the scatter fraction, that is, the fraction of scattered photons contained in the photopeak window, varies between ~25 and 40 %. Scattered photons will result in a loss of contrast in the image and poor quantification and hence must be corrected. SPECT scatter correction has been implemented using various "scatter" energy windows, convolution (blurring) techniques, sophisticated scatter model-based approaches [16–19] and by incorporating the estimated scattering into the iterative reconstruction algorithm. The simplest to implement are the energy window approaches, either the dual energy window [20] or triple energy window [21] methods. The algorithm that we developed, originally based on radionuclide transmission measurements and now based on CT data [22], is known as the transmission-dependent scatter correction (TDSC) algorithm [23]. TDSC is based on the convolution-subtraction model [24, 25] such that the scatter component of the image (g_s) is estimated by convolving the observed projection data (g_{obs}) with a scatter function (s):

$$\widehat{g}_s = k(g_{obs} \otimes s)$$

where the scatter fraction (k) scales the convolution to give the correct amount of scatter, which can then be subtracted from the observed data.

The scatter function (s) represents the response of a position sensitive detector to scattered radiation, which cannot be discriminated from the photopeak due to the limited energy resolution of the camera. The scatter function is generally evaluated by determining the response of the imaging system to a line source and modelled as a decreasing mono-exponential [23, 24, 26, 27] or as a combination of a Gaussian plus exponential functions [28].

An iterative approach to scatter correction was introduced by Bailey et al. [29], where the estimate of scatter is

Fig. 5 The steps involved in converting from a CT scan to linear attenuation map are shown. The threshold value t is usually chosen in the range 0–100 HU
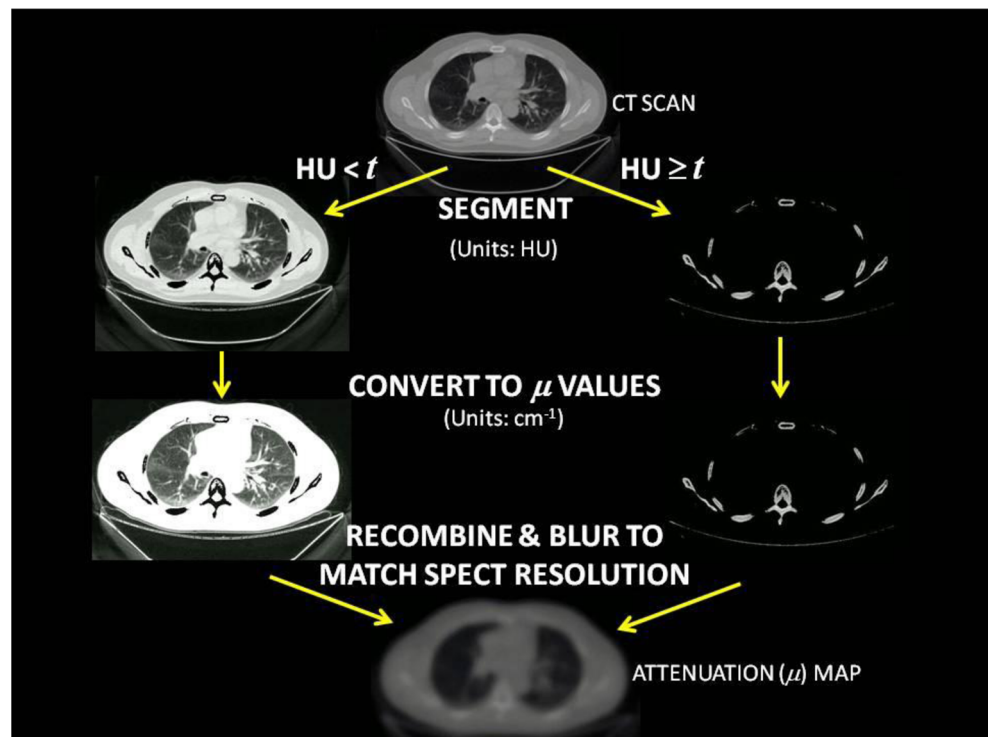
successively updated based on the corrected data calculated at each previous step. Ljungberg and Strand [30] demonstrated with Monte Carlo simulations that the scatter distribution is highly dependent on a particular object's density and geometry, leading to the introduction of a variable scatter fraction calculated for every point in the projection data based on radionuclide source-based transmission measurements [3, 23, 31, 32]. These pixel-by-pixel-based scatter fractions can be calculated from transmission data acquired simultaneously as the emission study or from ray sums through an attenuation map obtained from an alternative imaging modality, such as CT. Using the previous notation the TDSC method can then be expressed as:

$$\widehat{g}(x,y) = g_{obs}(x,y) - k(x,y)(g_{obs}(x,y)\otimes s)$$

where $\widehat{g}(x,y)$ is the estimated scatter corrected image and $k(x,y)$ is the matrix of scatter fractions derived from the transmission data. Scatter fractions can be calculated using empirical constants that represent the build-up function of the system [33]. Siegel et al. derived a generalised build-up function for geometric mean images which describes the build-up for a given attenuation path length μd:

$$A - B e^{-\mu \beta d}$$

As demonstrated by Meikle et al. [23], if the geometric mean of conjugate views is taken the scatter fraction per pixel can be written in terms of the measured transmission ($e^{-\mu T}$) and can be related to the build-up function as:

$$k = 1 - \frac{1}{A - B(e^{-\mu T})^{\beta/2}}$$

where the exponential term is equivalent to the transmission factor at a point and can hence be measured from transmission data. The constants A, B and β must be experimentally determined.

The TDSC method has been implemented by a number of groups today and shown, in combination with appropriate attenuation correction, to produce accurate quantitative SPECT reconstructions for a number of radionuclides [27, 28, 34–36]. The list of radionuclides investigated quantitatively with SPECT is already quite broad and includes ^{99m}Tc, ^{111}In, ^{123}I, ^{131}I, ^{177}Lu, ^{186}Re and ^{201}Tl.

Other corrections

While the correction for attenuation and scattered photons makes by far the greatest impact on quantification in SPECT, there are a number of other factors that need to be considered to produce quantitative images.

Dead time is usually not a major consideration when imaging with the gamma camera. Count rates are sufficiently low, even in dynamic planar studies, and historically dead time correction has not been applied to gamma camera data. However, when aiming for accurate quantitative images dead

time does need to be considered as it may constitute a small but necessary correction. It is typically of the order of 5 % in our experience when imaging [99m]Tc. An example of dead time response for ^{99m}Tc in scatter is shown in Fig. 6. Dead time may be much larger for certain applications of quantitative SPECT, such as imaging therapeutic doses of ^{177}Lu in the treatment of neuroendocrine tumours, which will contribute very high count rates, particularly at early time point imaging. In such circumstances, dead time correction is a necessity [37]. Gamma cameras typically do not measure dead time in real time, unlike PET cameras which are constantly monitoring count rate losses, and therefore a post hoc correction may be required [38]. It is important to remember that dead time in the gamma camera is affected by the detection of, and subsequent rejection of, scattered photons below the photopeak energy window and therefore any experiment that attempts to measure the dead time of a particular imaging system should include radioactive sources within a scattering medium approximating the clinical imaging situation. As gamma cameras become more quantitative for SPECT imaging, real time monitoring of dead time in the detector electronics may be required.

Another correction that is required is the conversion factor from the reconstructed image in counts per pixel to an image in units of radioactivity concentration per unit volume (kBq.ml^{-1}). In general, there are two approaches that can be implemented to derive this correction factor. Firstly, it may be possible to directly relate the reconstructed counts in the SPECT volume to the acquired counts in the projection data [22]. Calibration is then only related to an absolute value of camera sensitivity from the planar measurement under the
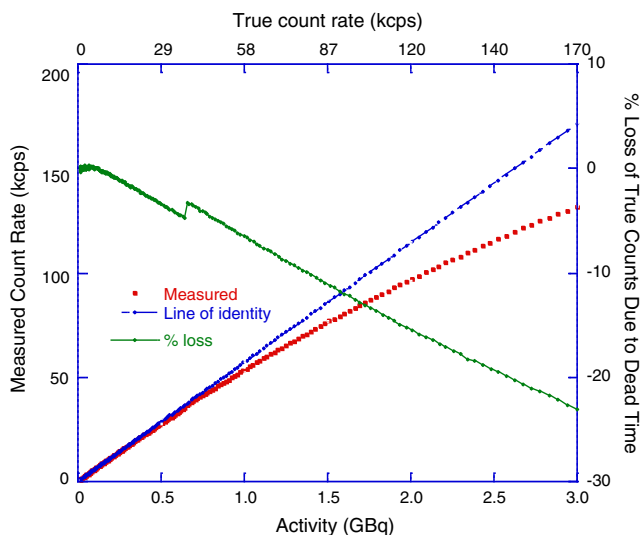
same imaging conditions in units of counts per second per kilobecquerel (cps/kBq^{-1}). The advantage of such an approach is that it is truly an absolute calibration and allows rigorous testing of the accuracy of the attenuation correction and scatter correction methods under various conditions. This is the method that we have employed in our laboratory as it provides the greatest insight into the accuracy of the various corrections.

The alternative approach is to use the method originally developed for PET imaging, where a cross-calibration factor (CCF) is determined from a reconstructed image relating reconstructed counts to radioactivity concentration [39]. This method was originally utilised in PET for a number of reasons: (1) as mentioned previously, attenuation correction in PET is straightforward and accurate, (2) in the earlier 2D PET systems the scatter fraction was sufficiently low so that it could be ignored and hence no scatter correction was required, and (3) determination of absolute sensitivity factor from a positron-emitting radionuclide source is not straightforward as there is the potential for positrons to escape from the solution and therefore not annihilating giving rise to the two photons that are detected. This can be mitigated by surrounding the positron-emitting source with a sufficient amount of attenuating material but this would then require a correction to obtain an absolute sensitivity value [40]. The measurement of an absolute sensitivity factor for PET was solved by the use of a device containing a number of attenuating "sleeves" of aluminium from which attenuation versus sleeve thickness was derived and extrapolated back to effectively no attenuation. This method was subsequently adopted by the National Electrical Manufacturers Association (NEMA) for the performance assessment of positron tomographs. The same approach can be used in SPECT. However, the cross-calibration approach depends both on accurate attenuation and scatter correction and is usually derived from a simple object such as a cylinder. The applicability of the cross-calibration factor to

Fig. 6 A plot of observed (*red*) vs expected (*blue*) count rates is shown for a dual-head gamma camera (SKYLight, Philips Medical Systems) for the geometric mean (GM) of opposing views when imaging a 20 cm diameter cylinder containing a decaying source of [99m]Tc. The percentage count rate loss is also shown (*green*). The discontinuity in the percentage loss curve seen at ~30 kcps is presumed due to the gamma camera's electronics changing the processing for count rates above this value

Fig. 7 The Siemens Symbia Intevo SPECT/CT system was introduced in mid-2013 as the first commercially available quantitative SPECT tomograph. It has calibration procedures and software applications for quantitative imaging with [99m]Tc (Symbia Intevo image courtesy of Siemens Healthcare and used with permission)

different geometries with varying attenuation, scattering and heterogeneous radionuclide distribution is a potential flaw in this approach. For this reason the absolute calibration approach is preferred if the reconstruction algorithm preserves the total counts acquired in the reconstructed volume; however, this is not always the case.

Finally, mention should be made of the poorer spatial resolution in SPECT compared to PET. Erroneous apparent decreases in the reconstructed radioactivity concentration due to limited spatial resolution is a problem when imaging objects which are less than approximately three times the spatial resolution of the imaging system. For SPECT, this could mean that objects less than 40–50 mm in size will be underestimated. Ad hoc corrections in the form of recovery coefficients applied to reconstructed data based on knowledge of the true size of the radioactive emitter (from CT) may be used to provide an estimate of true activity quantification in small structures [41]; however, such measures are cumbersome and depend on experimental modelling and the unlikely assumption of a spherical object. Distance-dependent resolution recovery algorithms may address some of this deficiency but it is an ongoing issue for SPECT quantification.

In spite of these limitations, SPECT/CT systems imaging ^{99m}Tc today report quantitative accuracy to within ±5 % of the true radionuclide concentration [42]. This is equivalent to the accuracy of current PET/CT systems.

Discussion

In this paper we have considered the main corrections necessary for quantitative SPECT reconstruction. Quantitative SPECT is a more challenging problem than PET as there are a greater number of variables to be considered such as different radionuclides with different photon energies, different collimators, potential for different energy windows to be used, and the potential for drifts in performance due to the greater number of moving parts in a SPECT system. In spite of the limitations, however, SPECT is gradually transitioning from purely qualitative image reconstruction to quantitative applications. A number of studies have now been published documenting validation of quantitative SPECT for ^{99m}Tc and ^{123}I in clinical scanning [22, 39, 43–45]. Further studies have been published using phantoms to validate a number of other radionuclides [37, 46]. It is particularly encouraging to see that one of the major gamma camera vendors has developed a quantitative SPECT system incorporating the corrections discussed in this paper suitable for imaging with ^{99m}Tc at present (Fig. 7). At this stage, as the system has not been released commercially and is still under evaluation, the quantitative accuracy that will be achievable in routine clinical practice and any limitations and regions of application remain unknown. It is likely, however, that quantification with other radionuclides will follow. It is anticipated that clinical applications for quantitative measurements using SPECT will follow the more widespread introduction of such systems. For a discussion of the requirements for implementation of quantitative SPECT and of potential clinical applications the reader is referred to a recent review article by the authors on this topic [42].

In summary, quantitative SPECT imaging holds promise due to some of the intrinsic advantages that SPECT enjoys compared to PET, namely the ability to perform multi-tracer studies simultaneously using different radionuclides, the generally longer physical half-lives of radionuclides lending themselves to measurements of temporally extended biological processes, the ready availability of radiotracers not requiring relatively close proximity to a medical cyclotron and rapid distribution network, and the lower cost of the systems and a much greater installed base worldwide than PET. While PET maintains considerable advantage over SPECT in terms of detection efficiency and spatial resolution, quantitative SPECT is likely to find a useful role in clinical nuclear medicine.

References

1. Pfeifer A, Knigge U, Mortensen J, Oturai P, Berthelsen AK, Loft A, et al. Clinical PET of neuroendocrine tumors using 64Cu-DOTATATE: first-in-humans study. J Nucl Med 2012;53(8):1207–15. PubMed PMID: 22782315. Epub 2012/07/12. eng.
2. Chang LT. A method for attenuation correction in radionuclide computed tomography. IEEE Trans Nucl Sci 1978;NS-25:638–43.
3. Bailey DL, Hutton BF, Walker PJ. Improved SPECT using simultaneous emission and transmission tomography. J Nucl Med 1987;28(5):844–51.
4. Shepp LA, Vardi Y. Maximum likelihood reconstruction for emission tomography. IEEE Trans Med Imaging 1982;MI-1:113–22.
5. Hudson HM, Larkin RS. Accelerated image reconstruction using ordered subsets of projection data. IEEE Trans Med Imaging 1994;MI-13(4):601–9.
6. Bailey DL. Transmission scanning in emission tomography. Eur J Nucl Med 1998;25(7):774–87.
7. Moore SC. Attenuation compensation. In: Ell PJ, Holman BL, editors. Computed emission tomography. London: Oxford University Press; 1982. p. 339–60.
8. Fleming JS. A technique for using CT images in attenuation correction and quantification in SPECT. Nucl Med Commun 1989;10:83–97.
9. LaCroix KJ, Tsui BMW, Hasegawa BH, Brown JK. Investigation of the use of X-ray CT images for attenuation compensation in SPECT. IEEE Trans Nucl Sci 1994;41(6):2793–9.
10. Brown S, Bailey DL, Willowson K, Baldock CA. Investigation of the relationship between linear attenuation coefficients and CT Hounsfield units using radionuclides for SPECT. Appl Radiat Isot 2008;66(9):1206–12.
11. Bailey DL, Roach PJ, Bailey EA, Hewlett J, Keijzers R. Development of a cost-effective modular SPECT/CT scanner. Eur J Nucl Med Mol Imaging 2007;34(9):1415–26. PubMed PMID: 17372731. Epub 2007/03/21. eng.
12. Beyer T, Kinahan PE, Townsend DW, Sashin D, editors. The use of X-ray CT for attenuation correction of PET data. IEEE Nuclear Science Symposium and Medical Imaging Conference. Norfolk: Institute of Electrical and Electronics Engineers; 1994.

13. Blankespoor S, Xu X, Kaiki K, Brown JK, Tang HR, Cann CE, et al. Attenuation correction of SPECT using X-ray CT on an emission-transmission CT system: myocardial perfusion assessment. IEEE Trans Nucl Sci 1996;43(4):2263–74.

14. Bai C, Shao L, Da Silva A, Zhao Z. A generalized model for the conversion from CT numbers to linear attenuation coefficients. IEEE Trans Nucl Sci 2003;50(5):1510–5.

15. Larsson A, Johansson L, Sundström T, Riklund-Ahlström K. A method for attenuation and scatter correction of brain SPECT based on computed tomography images. Nucl Med Commun 2003;24:411–20.

16. Beekman FJ, Kamphuis C, Frey EC. Scatter compensation methods in 3D iterative SPECT reconstruction: a simulation study. Phys Med Biol 1997;42(8):1619–32. PubMed PMID: 9279910. Epub 1997/08/01. eng.

17. Kadrmas DJ, Frey EC, Karimi SS, Tsui BM. Fast implementations of reconstruction-based scatter compensation in fully 3D SPECT image reconstruction. Phys Med Biol 1998;43(4):857–73. PubMed PMID: 9572510. Pubmed Central PMCID: 2808130. Epub 1998/05/08. eng.

18. Buvat I, Rodrigues-Villafuerte M, Todd-Pokropek A, Benali H, Di Paola R. Comparative assessment of nine scatter correction methods based on spectral analysis using Monte Carlo simulations. J Nucl Med 1995;36:1476–88.

19. El Fakhri G, Buvat I, Benali H, Todd-Pokropek AE, Di Paola R. Relative impact of scatter, collimator response, attenuation, and finite spatial resolution corrections in cardiac SPECT. J Nucl Med 2000;41(8):1400–8.

20. Jaszczak RJ, Greer KL, Floyd CE, Harris CG, Coleman RE. Improved SPECT quantification using compensation for scattered photons. J Nucl Med 1984;25:893–900.

21. Ichihara T, Ogawa K, Motomura N, Kubo A, Hashimoto S. Compton scatter compensation using the triple-energy window method for single- and dual-isotope SPECT. J Nucl Med 1993;34(12):2216–21. PubMed PMID: 8254414. Epub 1993/12/01. eng.

22. Willowson K, Bailey DL, Baldock C. Quantitative SPECT reconstruction using CT-derived corrections. Phys Med Biol 2008;53:3099–112.

23. Meikle SR, Hutton BF, Bailey DL. A transmission-dependent method for scatter correction in SPECT. J Nucl Med 1994;35(2):360–7.

24. Axelsson B, Msaki P, Israelsson A. Subtraction of Compton-scattered photons in single-photon emission computerized tomography. J Nucl Med 1984;25:490–4.

25. Msaki P, Axelsson B, Dahl CM, Larsson SA. Generalized scatter correction method in SPECT using point scatter distribution functions. J Nucl Med 1987;28:1861–9.

26. Msaki P, Erlandsson K, Svensson L, Nolstedt L. The convolution scatter subtraction hypothesis and its validity domain in radioisotope imaging. Phys Med Biol 1993;38:1359–70.

27. Kim KM, Varrone A, Watabe H, Shidahara M, Fujita M, Innis RB, et al. Contribution of scatter and attenuation compensation to SPECT images of nonuniformly distributed brain activities. J Nucl Med 2003;44(4):512–9.

28. Narita Y, Eberl S, Iida H, Hutton BF, Braun M, Nakamura T, et al. Monte Carlo and experimental evaluation of accuracy and noise properties of two scatter correction methods for SPECT. Phys Med Biol 1996;41:2481–96.

29. Bailey DL, Hutton BF, Meikle SR. Development of an iterative scatter correction technique for SPECT. Aust N Z J Med 1988;18:501. Abstract.

30. Ljungberg M, Strand S-E. Attenuation and scatter correction in SPECT for sources in a nonhomogeneous object: a Monte Carlo study. J Nucl Med 1991;32:1278–84.

31. Mukai T, Links JM, Douglass KH, Wagner Jr HN. Scatter correction in SPECT using non-uniform attenuation data. Phys Med Biol 1988;33(10):1129–40.

32. Ljungberg M, Strand S-E. Attenuation correction in SPECT based on transmission studies and Monte Carlo simulations of build-up functions. J Nucl Med 1990;31:493–500.

33. Siegel JA, Maurer AH, Wu RK, Blasius KM, Denenberg BS, Gash AK, et al. Absolute left ventricular volume by an iterative build-up factor analysis of gated radionuclide images. Radiology 1984;151:477–81.

34. Iida H, Narita Y, Kado H, Kashikura A, Sugawara S, Shoji Y, et al. Effects of scatter and attenuation correction on quantitative assessment of regional cerebral blood flow with SPECT. J Nucl Med 1998;39(1):181–9.

35. Kim KM, Watabe H, Shidahara M, Ishida Y, Iida H. SPECT collimator dependency of scatter and validation of transmission-dependent scatter compensation methodologies. IEEE Trans Nucl Sci 2001;NS-48(June):689–96.

36. Larsson A, Johansson L. Scatter-to-primary based scatter fractions for transmission-dependent convolution subtraction of SPECT images. Phys Med Biol 2003;48(21):N323–8.

37. Beauregard JM, Hofman MS, Pereira JM, Eu P, Hicks RJ. Quantitative (177)Lu SPECT (QSPECT) imaging using a commercially available SPECT/CT system. Cancer Imaging 2011;11:56–66. PubMed PMID: 21684829. Pubmed Central PMCID: 3205754. Epub 2011/06/21. eng.

38. Cranley K, Millar R, Bell T. Correction for deadtime losses in a gamma camera/data analysis system. Eur J Nucl Med 1980;5:377–82.

39. Zeintl J, Vija AH, Yahil A, Hornegger J, Kuwert T. Quantitative accuracy of clinical 99mTc SPECT/CT using ordered-subset expectation maximization with 3-dimensional resolution recovery, attenuation, and scatter correction. J Nucl Med 2010;51(6):921–8. PubMed PMID: 20484423.

40. Bailey DL, Jones T, Spinks TJ. A method for measuring the absolute sensitivity of positron emission tomographic scanners. Eur J Nucl Med 1991;18:374–9.

41. Hoffman EJ, Huang SC, Phelps ME. Quantitation in positron emission tomography: 1. Effect of object size. J Comput Assist Tomogr 1979;3(3):299–308.

42. Bailey DL, Willowson KP. An evidence-based review of quantitative SPECT imaging and potential clinical applications. J Nucl Med 2013;54(1):83–9.

43. Willowson K, Bailey DL, Bailey EA, Baldock C, Roach PJ. In vivo validation of quantitative SPECT in the heart. Clin Physiol Funct Imaging 2010;30(3):214–9.

44. Iida H, Nakagawara J, Hayashida K, Fukushima K, Watabe H, Koshino K, et al. Multicenter evaluation of a standardized protocol for rest and acetazolamide cerebral blood flow assessment using a quantitative SPECT reconstruction program and split-dose 123I-iodoamphetamine. J Nucl Med 2010;51(10):1624–31. PubMed PMID: 20847163. Epub 2010/09/18. eng.

45. Cachovan M, Vija AH, Hornegger J, Kuwert T. Quantification of 99mTc-DPD concentration in the lumbar spine with SPECT/CT. EJNMMI Res 2013;3(1):45. PubMed PMID: 23738809. Pubmed Central PMCID: 3680030.

46. Shcherbinin S, Celler A, Belhocine T, Vanderwerf R, Driedger A. Accuracy of quantitative reconstructions in SPECT/CT imaging. Phys Med Biol 2008;53(17):4595–604. PubMed PMID: 18678930. Epub 2008/08/06. eng.